For review purposes only

MICROSCOPY AND MICROANALYSIS

Determining projections of grain boundaries from diffraction data in the TEM

Journal:	*Microscopy and Microanalysis*
Manuscript ID	MAM-15-220.R1
Manuscript Type:	Original Article
Date Submitted by the Author:	11-Jan-2016
Complete List of Authors:	Kiss, Ákos; Center for Energy Research; Institute for Technical Physics and Materials Science Lábár, János; Center for Energy Research; Institute for Technical Physics and Materials Science, ; Eötvös Loránd University, Dept. of Materials Physics
Keywords:	grain boundary plane, non-negative matrix factorization, electron diffraction, computer program, polycrystalline thin films

SCHOLARONE™
Manuscripts

Determining projections of grain boundaries from diffraction data in the TEM

Ákos K. Kiss[1, 2] and János L. Lábár[1*]

[1] Hungarian Academy of Sciences, Research Center for Energy Research, Institute for Technical Physics and Materials Science (MTA EK MFA), Konkoly Thege M. út 29-33, H-1121 Budapest, Hungary

[2] Doctoral School of Molecular- and Nanotechnologies, University of Pannonia, Faculty of Information Technology, Egyetem u. 10, H-8200 Veszprém, Hungary

For Peer Review

Keywords: grain boundary plane, non-negative matrix factorization, electron diffraction, computer program, polycrystalline thin films

[*] Corresponding author: labar@mfa.kfki.hu

GB-plane projection width from diffraction data

Abstract

Grain boundaries (GB) are characterized by disorientation of the neighboring grains and the direction of the boundary plane between them. A new approach presented here determines the projection of grain boundaries that can be used to determine the latter one. The novelty is that an additional parameter of GB-s is quantified in addition to the ones provided by the orientation maps, namely the width of the projection of the GB is measured from the same set of diffraction patterns that were recorded for the orientation map, without the need to take any additional images. The diffraction patterns are collected in nanobeam diffraction (NBD) mode in a transmission electron microscope (TEM) pixel-by-pixel from an area containing two neighboring grains and the boundary between them. In our case the diffraction patterns were recorded using the beam scanning function of ~~the~~ a commercially available ~~ASTAR~~ system (ASTAR). Our method is based on non-negative matrix factorization (NMF) applied to the mentioned set of diffraction patterns. The method is encoded in a MATLAB environment, making the results easy to interpret and visualize. The measured GB-projection width is used to determine the orientation of the grain boundary plane, as given in ~~Microsc. Microanal. 21, 422–435~~Kiss et al., 2015.

For Peer Review

Introduction

The macroscopic properties of a GB are described by 5 parameters (5 degrees of freedom): 3 of them stand for the misorientation and 2 others describe the orientation (i.e. the normal vector) of the crystallographic plane of the grain boundary (GB) between them (Randle, 1993). In that description even curved GBs are approximated locally by planes. That approximation is valid even for GBs with significant curvature (Forwood & Clarebroug, 1991). The orientation of any individual grain means the relation between its native crystallographic system and the free chosen laboratory coordinate system i.e. corresponds to a coordinate-transformation. The misorientation between two grains is defined as a rotation

For review purposes only

transformation between the two Cartesian coordinate systems attached to the native crystallographic systems of the neighboring grains so it is deduced from the orientation matrices. Although the well-known coincidence site lattice theory (CSL-theory) is widely used for characterizing polycrystalline samples, it only describes the misorientation of the neighboring grains for special low energy arrangements (Grimmer et al., 1974) and does not specify the orientation of the boundary plane between them.

Determination of the orientation of the boundary plane is more tedious than the determination of the orientations of the grains. Such measurements are frequently carried out in scanning electron microscopes (SEM) using electron backscatter diffraction (EBSD) or electron channeling patterns (ECP) (Lloyd et al., 1997). In the simplest version of the EBSD method an orientation map of the grains is recorded and the directions of the surface line traces of GBs are identified. Since the inclination of the GB plane is not identified and a large number of GB orientations can result in the same surface line trace, the method gives an incomplete characterization of the GB (Saylor et al., 2004). However, knowledge of the direction of the surface line trace of the GB-plane alone can be used to decide whether the GB can be a special one or not (e.g. in case of Σ3 misorientation: can the plane of the GB be {111}-type or not.) (Randle, 2001). For complete characterization a tedious 3-dimensional (3D) EBSD approach is needed. After an EBSD map ~~was~~ has been recorded, a very thin layer of fixed thickness is removed (parallel to the original surface) either by mechanical polishing or by a Focused Ion Beam (FIB). These two subsequent steps are cycled and the virtual shift of the GB line traces as a function of depth ~~is followed~~follows. Thus the 3D distribution of boundaries can be reconstructed (Saylor et al., 2003, Zaefferer et al., 2008).

For Peer Review

In our previous work, we showed a complete characterization of GBs with a semi-automatic procedure in the TEM (Kiss et al., 2015). It is based on a combination of orientation maps and bright field (BF) images in the TEM. Although that approach is easier than the one applying

the 3D EBSD / FIB technique, it cannot be completely automated and concentrates only on a small number of boundaries at a time. In the present paper, we eliminate the need to collect BF images and ~~will~~ extract both the orientations of the grains and the orientation of the grain boundary from the same diffraction patterns only. It is regarded as a first step towards complete automation.

Our approach performs measurements viewed from at least two orientations of the sample. It uses directly the information encoded in the differences in the diffraction patterns originating from the neighboring grains. Our method works best in orientations far from strong diffraction conditions, where only weak thickness related dynamic effects are present (i.e. no strong thickness fringes are seen in the overlapping area). The width and the direction of the projection of the GB plane between two crystallites can be determined from the diffraction patterns (irrespective of the crystal structures and the orientations of the grains). Whenever the GB plane is oriented oblique to the electron beam, the overlapping area of the neighboring grains is discerned and ~~using the known local thickness of the thin film~~ the inclination of the GB plane can be deduced from the measured projected width of the GB (Kiss et al., 2015) using the known local thickness of the thin film.

For Peer Review

There are various ways to determine the local thickness of the investigated area (Kelly, 1975; Egerton, 2011; Stadelmann, 1987; Pozsgai, 1997). Since we aim at developing a method that can be used for GB plane analysis in a wide area, the thickness measurements ~~are preferred, which~~ that provide thickness information over a large area (e.g. ~~EELS~~ thickness mapping by electron energy loss spectroscopy, EELS) are preferred. In the preferred case a lamella prepared by focused ion beam (FIB) is used with known constant thickness.

Although the thickness of the sample was a necessary input parameter in our previous measurements (Lábár et al., 2012, Kiss et al., 2013), we showed that the thickness can also be determined simultaneously to the measurement of the GB-projections (Kiss et al., 2015).

GB-plane projection width from diffraction data

Non-negative matrix factorization in brief

Statistical methods, such as principal component analysis as well as non-negative matrix factorization (NMF) have ~~a wide range of~~ applications in different kinds of disciplines ~~e.g. in~~ ranging from biology (Sotiras et al., 2015, Brunet et al., 2004)~~, nuclear sciences or in~~ to computer science~~s~~ (e. g. signal processing and pattern recognition; Smaragdis et al., 2003, Buciu et al, 2004). Devarajan's work focuses on the field of computational biology, however it also gives a remarkable outlook to the capabilities of NMF-analysis (Devarajan, 2008). Each of these applications aim~~s~~ at handling a big amount of (measured) data by revealing its main building blocks by matrix decomposition. In the field of material sciences Eggeman, Krakow and Midgley have shown the impressive possibilities of the application of NMF. They revealed and reconstructed the 3D-microstructure of a Ni-base superalloy by combining electron tomography, precession electron diffraction and NMF techniques (Eggeman et al., 2015). However, the method described in our paper reveals the GB in the third dimension (by giving its direction) without the need of any special TEM-holders developed for tomography. All of our measurements were carried out by a frequently used double-tilt holder with a tilt-range no bigger than ±15°.

For Peer Review

The non-negativity is a quite strong, but useful constraint for data matrix factorization that can discover a “building-block” representation of data ~~formed by~~comprising non-negative values (such as intensities measured by CCD cameras). Berry et al. give a good summary of the main algorithms of numerical NMF and their historical development, emphasizing that the works of Paatero ~~should~~ deserve more attention than what they receive, in contrast to the most cited work of Lee and Seung (Berry et al., 2006; Paatero & Trapper, 1994, Lee & Seung, 1999). However, Lee and Seung give a very illustrative description and “comparison of vector quantization, principal component analysis and non-negative matrix factorization” in their aforementioned work.

GB-plane projection width from diffraction data

Applying NMF on **V** non-negative matrix, **W** and **H** non-negative matrices are generated, where:

(eq.1) $\boldsymbol{V} \approx \boldsymbol{W} \cdot \boldsymbol{H}$

Note, that this factorization is not unique: when **D** is an invertible non-negative matrix, $\mathbf{D}^{-1}$ is also non-negative. Then $\boldsymbol{V} \approx \boldsymbol{W} \cdot \boldsymbol{H} = \boldsymbol{W} \cdot \boldsymbol{D} \cdot \boldsymbol{D}^{-1} \cdot \boldsymbol{H} = \boldsymbol{W}' \cdot \boldsymbol{H}'$.

Consider we have *m* measurements (such as diffraction patterns), each measurement holds *n* parameters (such as pixel intensities) i.e. each measurement is represented by an *n*-dimensional column-vector. The **V** data matrix with the size of *nxm* contains each measurements in its columns. Let be **W** and **H** matrices with size of *nxk* and *kxm* respectively. Thus, taking the corresponding column **h** from **H** and **v** from **V**:

(eq.2) $\boldsymbol{v} = \boldsymbol{W} \cdot \boldsymbol{h}$

This implies that each column in **V** arises as a linear combination of datasets presented in the columns of **W** with the weight factors in **H**. In other words, each example in the columns of **V** data matrix is expressed with the help of *k* pieces of non-negative base components stored in the columns of **W**.

The exact mathematical problem according to (eq.1) can be formulated differently, depending on the way how one defines the “distance” between two matrices. (Lee & Seung 2001). Each formulation aims at minimizing this “distance” between **V** and **W**·**H**. Also there are different algorithms solving the aforementioned minimization (Berry et al., 2006). In our work, we applied the algorithm of projected gradient method for NMF presented by Chih-Jen Lin (Lin, 2007). Due to its good convergence, this algorithm works much faster than the multiplicative method presented by Lee and Seung (Lee & Seung 2001). Thus a GB can be evaluated in 5 or 10 minutes (depending on the number of measured points).

GB-plane projection width from diffraction data

Application of NMF to diffraction data

Initialization and calculation of the weight factors

In order to generate an orientation map in a TEM with the help of the ASTAR system, thousands of diffraction patterns are taken position-by-position in the scanned area of interest. The probe size and the step size must be adjusted to each other. They together determine the resulting pixel size in the final orientation map. Though the grains and the net of GBs are possible to identify in the orientation map, we have no information about the extension of the overlapping areas between the grains. At this point the role of the "reliability-index" has to be mentioned. The ASTAR system is forced to assign an orientation to each position (of the area scanned on the sample) from the diffraction pattern taken at that position. When a position lies in the overlapping area, its diffraction pattern contains spots coming from both of the neighboring grains, thus the exact orientation represented by this position can be hardly specified. Therefore the "reliability-index" decreases in the overlapping area. Thus eventually the line of the boundary shows up clearly on the orientation map, as well as the "reliability-index" may suggest that there is a significant overlap. However the width of the projection cannot be characterized with help of the "reliability-index" (see ***Fig. 1*** – the scanned area shown here is the same, as it is presented and evaluated later in the "2nd example").

For Peer Review

Our aim is to detect and measure the width of the chosen GB-projection, therefore the local neighborhood of the parts of GB, where only two of neighboring grains are present, is analyzed by NMF. (Any GB section in a GB-network of a polycrystalline sample has only two neighboring grains. Triple junction areas are not considered here.) The dataset to be analyzed is formed by the set of diffraction patterns stored in the area of the chosen neighborhood. The expected base components are the two kinds of diffraction patterns coming from the two individual grains – this is why the input-parameter of the factorization-

algorithm, which pre-sets the number of base components, is set to 2 (this parameter was referred to by k in the previous chapter). Since the measured values i.e. the intensities in each diffraction pattern are non-negative, NMF perfectly fits to our studies.

The matrices of (eq.1) are as follows:

V – data matrix, with ~~the~~ size ~~of~~ equals to $n x m$. Each column of **V** contains the intensity values stored in the diffraction patterns, m is the number of the diffraction patterns (i.e. the number of probed positions) being present in the scanned region (typically more than ten thousand), n is the number of pixels in a single diffraction pattern, i.e. intensity values stored in any diffraction pattern (in our case: n=144x144=20736).

W – base component matrix with the size of $n x 2$. The two columns represent the calculated diffraction patterns, which belong to either of the neighboring grains, respectively. At the beginning of the NMF-evaluation they are initialized by the measured intensities coming from the centers of gravity of each side of the GB to be evaluated (as it will be discussed later, a prior estimate of the trace of the GB is known from the orientation map).

H – weight factor matrix with the size of $2 x m$. The two rows contain the weight factors of the base components. The pair of weight factors in each column of **H** belong to the same column in the data matrix – see ***Fig. 2***. Its values are initialized by random numbers.

In the next chapter real experimental examples are presented, where the GB-plane is determined (indexed) with the help of NMF evaluations. In ***Fig. 3/a, b*** acquired diffraction patterns are shown coming from an area containing an investigated GB and large parts of its two neighboring grains. ***Fig. 3/c, d*** show the calculated base components (these data came from our *"2nd example"* at the tilt case of -1° / -14.2°). As it is expected, their matching is significant and obvious, since the calculated components were initialized by the corresponding measured ones. (It is clearly seen that the central spot is omitted from the

For Peer Review

calculated data. This will be discussed later in the chapter "Limitations of the method".) At this point it is worth mentioning, that the proper initialization guarantees that the proper components are found (since the NMF-algorithm is based on an extreme value problem), yet the application of the NMF itself makes a room for the refinement and precise finding of the base components (as it is the case in slightly bended samples or at the presence of any dirt).

Using the weight factors along a GB to measure the width of the projection

Together with the identification of the base components, the weight-factors related to them are calculated at each mapped position. In ***Fig. 4*** the typical trends of the calculated weight-factors (related to one of the neighboring grain) are plotted as a GB is crossed along a line. After the weight factors had been calculated, they can be displayed pixel-by-pixel in the studied area. The lateral distribution of these weight-factors serves as a basis of the automated detection of the overlapping area (i.e. the projection of the investigated GB) between two neighboring grains and of the measurement of its projected width. These weight factors can be visualized with the help of contour levels, as we will present them in the next chapter (see ***Fig. 7***, ***Fig. 8***).

Plotting the weight factors along a line normal to the GB trace (as in ***Fig. 4***) assumes that we have prior knowledge about the direction of the GB trace. This information is preliminarily deduced from the orientation map: the NMF analysis of a boundary is carried out just after its approximate trace is determined from the orientation map when the diffraction data from the boundary and the neighboring grains are collected. In the ideal scenario, the weight factors along a section crossing the boundary form a step function between 1 and 0 with a linear transition interval: the width of the transition-part is determined by the width of the GB.

However, cases are also encountered, in which the transition part shows strong non-linearity – the reasons of this is mainly dynamic diffraction, as detailed in the section "Limitations of the method". In practice, strong diffraction conditions can be avoided by properly orienting the

For Peer Review

sample, but a slight non-linearity at the transition has to be taken into account anyhow. This is why we do not approximate the transition part by a single line only, but by two line segments. The weight factors along a section perpendicular to the GB are split into the "left side" and the "right side" of the boundary: the division point is the middle point of the transition-part defined by the mean value between the minima and the maxima of the weight factors. Therefore, each "side" of the boundary contains two linear parts: one belonging to one of the neighboring grains and another~~, which belongs~~ belonging to the transition region (projection of the GB). Our goal is to find the "break-point" between these parts in each "side" of the boundary. ***Fig. 4/a, b*** show examples of cross-sections: the weight factors in ***Fig. 4/a*** represents a nearly ideal GB, in ***Fig. 4/b*** the transition part has significant curvature, but our algorithm can also handle a case like this. Diffraction patterns along multiple parallel lines, normal to the boundary, are evaluated. Multiple sets of "break-points" are identified in those multiple lines. These ~~many~~ "break-points" ~~together~~ define the edges of the GB-projection, making possible to refine the direction of the GB-trace and to measure the width of the GB-projection.

Once a section is chosen and its "left side" and "right side" ~~is~~ are identified, the "break-points" are found by a brute-force method. On each side, the line fitting is carried out for all the possible positions of the "break-point" and the accepted position is the one, where the sum of the residuals is minimal.

The width of the GB-projection along a given line is given by the distance between the pair of "break-points": since our algorithm defines the "break-points" as the nearest pixels, which are not part of the transition area, the width expressed in nanometers is given by *step_size [nm] * (difference_in_the_indexes_of_the_break_points - 1)*.

For Peer Review

For review purposes only

GB-plane projection width from diffraction data

Eliminating irregular data points

Although the majority of the parallel lines define the same width for the projection of the GB (that is normal to these parallel lines), occasionally some points are outliers (e.g. at locations where significant bending of the sample occurs or at locations where artefacts, e.g. dirt are being present by chance on the sample). Such rare outlier points are excluded from the evaluation of the average GB width. Outlier points (are easily identified visually, however, they) are identified automatically by fitting lines on each side of the GB with a fixed direction predetermined from the orientation map. We calculate the standard deviation (σ_d) of the distances of the break-points from the fitted line: the points lying out of $2\sigma_d$ are excluded. All pairs of break-points are excluded from the final calculation of the average and standard deviation, where at least one of them is an outlier.

The resulting "break-points" are the basis for refining the direction of the GB-trace by unconstrained line fitting. The pairs of break-points determine individual width-values along the trace of the GB. Their mean is considered as the width of the GB-projection; their standard deviation contributes to the random error of the measurement. Although fitting a common line to the GB-edges and calculating the distance between these fitted lines might seem to be useful in width-estimation, we follow a different procedure due to two effects. First, the "break-points" may not lie on a straight line – even a slight curvature of the GB-edges would introduce a significant error in such a width-measurement. Second, any drift during the diffraction pattern acquisition alters the orientation of the observed trace and would also introduce error in the measurement. This is why only individual width-values coming from the subsequent lines are taken into account individually and consolidated into a single value in the last step.

For Peer Review

GB-plane projection width from diffraction data

Determining both the direction of the GB-plane and local thickness from the obtained projected widths

The 3D orientation of the GB-plane is determined from the measured projected width of the GB, the 2D orientation of the GB-trace and the local thickness of the sample (Kiss et al., 2015). Since both a "left"-tilted and a "right"-tilted GB-plane can produce the same projected width, an ambiguity appears in the calculation. In principle, this ambiguity can be resolved by combining two measurements at two goniometer tilt values. Since we had multiple measurements at multiple tilts in each examples presented in this paper, we applied curve fitting instead of a pair-by-pair evaluation. The projection (p_i) of a chosen GB-plane as a function of the ith tilt (α_i) around a sample holder axis can be described by (eq. 3):

(eq. 3) $p_i = d \cdot \cos(\alpha_i + \omega) = d \cdot \cos\omega \cos\alpha_i - d \cdot \sin\omega \sin\alpha_i = A \cdot \cos\alpha_i + B \cdot \sin\alpha_i$

Where: d – "real" width of the GB-plane section within the sample, measured between the two surfaces of the thin film, ω – GB-plane inclination, measured from the sample surface.

To find d and ω, the easiest way is to apply linear fitting to the measured p_i values against the corresponding values of $\sin(\alpha_i)$ and $\cos(\alpha_i)$ (see eq. 3). The fitting has been carried out in two steps. The rough estimate given by the "LINEST" function of Microsoft Excel served as input to the iteration in the OriginPro 2015 software – the final values and standard deviations of the parameters are calculated by weighted linear fitting with the help of the Origin software.

A demo version of the new software is available from

http://www.thinfilms.hu/downloads.html.

Application examples

Validation by comparing to manual method

A LASER crystallized silicon thin film with the thickness range of 135 nm (± 10 %) has been investigated in order to present the capabilities of the NMF-method. A JEOL JEM 3010

For review purposes only

GB-plane projection width from diffraction data

HRTEM operated at 300 kV was used with a ± 15° double tilt sample-holder. The main axis and the goniometer axis of the holder points into the directions of -162.5° and -72.5° in the image plane, measured from the direction pointing right in the image. Calibration of these values ~~are~~ is essential for calculating the tilt position of the sample regarding to the GB: we do not use the whole misorientation coming from the absolute values of the tilt positions, only the tilt about the axis parallel to the observed GB-projection is important, because any further tilt about an axis lying perpendicular to the GB-trace has no impact on the width/direction of the projection (Kiss et al., 2015).

In our former work, the same group of Si samples has been investigated and a relation was shown between the type (energy density) of the GB-planes and the distribution of their inclination angles measured from the sample surface (Kiss et al. 2013, Lábár et al. 2012). The Si thin film shown here has been LASER crystallized from an amorphous layer then it was transferred onto a TEM grid after the substrate had been etched away. The LASER crystallization resulted in crystals with lateral size of 400-600 nm or even bigger. Lot of coherent twin lamellae are present with ∑3 misorientation and {111} type GB plane, also with wide angular distribution measured from the sample surface. Our Si film is thick enough to characterize GBs through their projections, as well as the structure of the sample makes easy to find low-index boundaries: these conditions make this sample ideal for testing our method.

For Peer Review

In our former work, we characterized some GBs manually one-by-one making the data-collection very time-consuming. The experimental conditions had to be optimized for human operation therefore every measurement needed special patience and practice of the TEM-operator. In the case of manual characterization, the sample had to be tilted to an orientation, where the projection of the GB-plane produced sharp contrast in the image. This was carried out by tilting one of the neighboring grains in two-beam condition resulting in thickness

fringes in the overlapping (double-wedge-shaped) area between the grains (see ***Fig. 5/a,b,c*** and ***Fig. 6/a,b,c***). The lengthy and complicated nature of manual operation stimulated us to the development of the present method, which eliminates the need for recording images in addition to the diffraction patterns used to determine the orientations. The validation of the new procedure is done by comparing the present results with the results of the previous, manual operation. It is shown that our new procedure, which relies on less experimental input, gives the same projection widths within the experimental error with acceptable reliability as the more tedious manual method.

For Peer Review

Two examples are presented here on the same Si film: coherent twin boundaries with different inclinations have been evaluated both "manually" and with the help of NMF analysis. The new method also starts with collecting orientation maps from the area of interest in multiple tilt conditions. All steps of the further evaluation process are based on computer-implemented algorithms without the need for recording images, unlike in the manual procedure. Both examples show good agreement between the results of the "manual" and NMF methods.

Different sensitivity to error as a function of diffracting condition and scan-direction

It has turned out during our measurements that an NMF analysis on patterns recorded at two-beam condition produce artefacts (see chapter "Limitations of the method"). Consequently, the orientation maps were collected at goniometer tilt values different from where the images were taken for the "manual" evaluation. ***Fig. 5*** and ***Fig. 6*** shows the tilt positions chosen for the different types of evaluation: sharp thickness fringes (due to strong diffraction) are seen on the BF images taken for "manual" measurements (***Fig. 5/a,b,c*** and ***Fig. 6/a,b,c***) and no contrast of the boundary-plane was present at all at the same part of the GBs, when they were set in non-specific tilt positions (away from any strong ***diffracting condition***) for NMF

GB-plane projection width from diffraction data

analysis[1] (***Fig. 5/d-g*** and ***Fig. 6/d-g***). The orientation maps were collected in these later goniometer tilt positions from the chosen boundary: the mapped area is 500 nm *500 nm, the beam size and the step size of the scan is 10 nm and 5 nm respectively. NMF was applied on the collected sets of diffraction patterns. As a result, ***Fig. 7*** and ***Fig. 8*** show the contour-level visualization of the weight factors related to one of the neighboring grains. The overlapping area can be recognized very clearly, where the contour lines run densely and parallel to each other. The resulted "break-points" are marked by filled, different symbols (triangle and circle, each for one side) and the excluded points are marked by empty symbols. The predetermined direction of the GB-projection is indicated by the straight lines, which are the basis of finding the outliers. In both of our examples, the width values have the same (*positive*) sign, in accordance with that, none of the tilts has turned any of the chosen boundary planes from "left" to "right" tilted position or vice versa.

A special type of experimental error, namely the mechanical drift of the sample holder in the TEM, also proved to be a limitation to our accuracy, so we selected two examples here to demonstrate its effect and to highlight our limits. We also show in these two examples below that proper selection of the scan direction can minimize that error. Since the scan direction can be set arbitrarily, the ***scan direction*** was set parallel to the trace of the GB in the ***first*** example. This arrangement ensured that either the apparent direction of the GB-projection or the measured width of the GB-projection ~~is~~ are the least affected by the drift. The ***second*** example is selected to produce the largest possible error due to this effect, namely the scan direction is set perpendicular to the trace of a GB, which also happened to be perpendicular to the drift direction. To reduce the effect of drift on the measured width of the GB-projection, the individual scanned lines are evaluated individually. Since the scanning beam resides over

[1] The BF images in ***Fig 5/d-g*** and ***Fig. 6/d-g*** were not needed for the evaluation. They were only recorded to demonstrate that the diffracting effect is missing from the image in these goniometer tilt directions.

For Peer Review

the overlapping area only for a short time in each line – in this short time a sample-drift cannot develop any significant effect on the measured width. The drift between the individual lines is neutralized by the separate evaluation of each line. The widths measured over the individual lines are consolidated statistically in the final step. This is why we emphasize that only the direction of the GB-trace may be affected by the drift, however this effect can be controlled by properly choosing the ***scan direction***. However, the apparent direction of the projected GB is the most distorted when the drift is normal to the GB-trace and this error is not eliminated by the normal scan direction. Altogether, the smallest error is expected in the "*1st example*" and most of the error in "*2nd example*" is originating from a distortion of the apparent direction of the 2D GB-trace.

For Peer Review

1st example; minimal effect of drift

The experimental parameters and the primarily determined quantities ~~measured and resulted data~~ are summarized in ***Table 1*** and ***2*** for the case when the scan direction is parallel to the GB. It is clearly seen on ***Fig.*** *7*, that the accuracy of the edge-detection of projection may vary with the goniometer tilt position i.e. diffraction condition, even if it is far from any two-beam conditions. The curves fitted to eq. 3 for both the measured and NMF-evaluated data of this example are shown in ***Fig. 9.a***. On ~~the~~ average, the results from manual- and NMF-analysis are in good agreement in this example: both of the methods gave an average solution for the GB-plane close to the same {111}-type boundaries within the rage of a few degrees. This is in accordance with the expected good accuracy of our results in this example. (The reader is reminded that the accuracy of the input data is about 1°.) Accuracy could be improved in a TEM with larger allowed goniometer tilt values.

2nd example; maximal effect of drift

For the scan direction perpendicular to the GB, the measured and the resulted data are detailed in ***Table 3*** and ***4***. The curves fitted to eq. 3 for both the measured and NMF-evaluated data of

this example are shown in ***Fig. 9.b***. ***Table 4*** shows that the directions of the resulted GB-planes calculated by the two different methods are relatively "far" from each other. (The origin of the error is identified to be the drift, since we found the same angular difference between the traces of the planes as the difference in angles between the resulted GB-planes – as seen in ***Fig. 6/a-c*** and in ***Fig. 8***). This significant error is introduced by a 2-3 nm/min sample drift in horizontal direction during the diffraction-data acquisition, which took 30-40 min per measurement in our examples. The sample-drift could noticeably influence the result (i.e. the apparent direction of the GB trace) in this example, since the trace of the GB runs perpendicular both to the direction of the drift and to the direction of the beam-scan, so the consecutive lines are shifted by the drift value characteristic of the time of scanning over one line. This is why we emphasize that the well selected scanning-direction during the data acquisition may increase the reliability of the evaluation, as ~~it is presented~~shown in our previous example. The separate evaluation of each line can neutralize the drift effect in the measured value of the projection width, but cannot neutralize the distortion caused in the apparent direction of the trace of the GB.

The values of the inclination angles and the direction of the GB-trace are important parameters for the characterization of the GB-planes, however, only the direction of the GB-trace can be influenced by any drift. This is in accordance with the fact~~,~~ that the inclination angles show much better agreement (between the two methods) than the direction of the traces of the GBs. This is true for both of our examples. We can conclude that the error introduced by the drift is significant~~,~~ when the GB-trace runs perpendicular to the drift (see "2nd example") and it is negligible when it is parallel to that (see "1st example"). However, the impact of the drift can be moderated when the scan-direction of the mapping is chosen to be parallel to the GB-trace, even when the trace is perpendicular to the drift. In such an experimental condition the scanning beam resides over the most important overlapping area

GB-plane projection width from diffraction data

only for a ~~few~~ small percent of the overall scanning-time – in this short time the drift cannot develop any significant effect.

Limitations of the method

Diffraction and other experimental conditions

Since we are interested in the variation of the diffraction signal when crossing the GB, it is fundamental to optimize the experimental conditions during the data acquisition. In order to have the best results, the following~~s~~ have to be considered:

- The scanning spot size and the step size have to fit to the features of the investigated sample: several spots have to lie within the overlapping area. The spot size contributes to the systematic error and the step size specifies the lower limit of the random error. In our case the step size is the half of the probe size.
- Although one tries to increase the signal-to-noise ratio by increasing the recorded intensity, the saturation of any diffraction spots has to be avoided in order to decrease non-linearities~~y~~ as much as possible. Since the direct beam always saturates, it is cut off from the diffraction patterns to be evaluated: the pixels belonging to the direct beam (i.e. in a disk with pre-set radius) are set to zero.
- The diffraction patterns have to be stably positioned, i.e. unexpected small electrical drift of the TEM's projection system causing lateral shift of the diffraction pattern have to be corrected after the data acquisition. We assume that only the direct spot has saturated pixels in the diffraction patterns: the center of gravity of the saturated pixels is located and compared to the pre-set, nominal center of the diffraction pattern. A lateral shift is applied to each pixel in order to bring the center of the direct spot back in the middle of the diffraction pattern (the typical range of this shift is 0 to 4 pixels in

For Peer Review

our examples). Therefore a continuous drift is compensated by discrete shifts. The sensitivity of the NMF analysis is well presented in this point: a significant jump artefact may occur in the weight factors if the correction is not accurate enough. Thus it is crucial to carry out the centering with sub-pixel resolution (in our cases with 0.2 * *pixel_size*). Linear interpolation is applied on each diffraction data in order to increase the resolution. After the centering has been applied on the interpolated data, the final diffraction pattern is generated by sampling with the original resolution.

It is an advantage of the method that no special diffraction condition is needed for the best results. However, we found that the strict two-beam condition in any of the neighboring grains may result in a completely false "measured" projection width. In the early stages of our experiments diffraction patterns were evaluated, which were acquired in special orientation conditions to have sharp thickness fringes in the BF images from the overlapping area. However, the weight factors in the overlapping area were dominated by the dynamic effect (oscillating intensity) rather than "switching" from the one grain into the other. The direct beam is omitted from the analyzed diffraction data therefore the weight-factors are determined only by the diffracted beam(s). Since the intensity of the diffracted beam(s) oscillates, the weight factors show strong false non-linearity in the transition area making the detection of the GB-projection highly inaccurate or even impossible (see ***Fig. 10***). That is why strong diffracting conditions have to be avoided in the experiments.

Error analysis

Since the position of the GB is arbitrary in the scanned area, the accuracy of the width estimation of the GB projection is determined in general by the standard deviation of the resulting width-values along the GB (σ_{GB} – this is calculated after omitting the excluded points) and the step size (s), which depends on the direction of the GB (α, measured from the

For Peer Review

axis pointing to the right). The "effective step size" (s_{eff}) covers the step size perpendicular to the direction of the GB-projection.

(eq. 4)

$$if\ \alpha \geq 45° : s_{eff} = s \cdot |\sin \alpha|$$

$$if\ \alpha \leq 45° : s_{eff} = s \cdot |\cos \alpha|$$

The systematic error of the width measurement corresponds to the beam size (*b*). The random error varies between *0* and $2 \cdot s_{eff}$, and uniform distribution is considered due to the random position of the GB – its standard deviation (σ_s) holds the contribution to the resulting random error. Thus the width (*d*) is deduced from the width of the transition part (d_t) as follows:

(eq. 5)

$$d = (d_t - b - s_{eff}) \pm \sqrt{{\sigma_s}^2 + {\sigma_{GB}}^2}$$

The error values for the NMF-calculation of width given in ***Table 1*** and ***Table 3*** are calculated by (eq. 5). Since these values have a lower limit determined by the step size, and also depend on the actual diffraction condition (which is responsible for σ_{GB}), GB-plane calculation based on two-measurements can be carried out with reasonable accuracy only when the data are collected in significantly different tilt positions (10°-15° in difference at least) and the sample is off from strong diffraction conditions. Only when the aforementioned experimental conditions are realized, the inclination of the GB can be estimated within the accuracy of ±5°. This is in agreement with the error estimation described in (Kiss et al., 2015), where the relation between error-propagation and the input tilt-conditions are discussed. The relatively high inaccuracies of the NMF-analysis can be compensated by collecting data in multiple tilts and applying curve-fitting. We emphasize, that a sufficient tilt series can be collected even with relatively low tilt possibilities (±15°).

For Peer Review

For review purposes only

GB-plane projection width from diffraction data

Conclusions

A powerful statistical method, the non-negative matrix factorization (NMF) was applied to sets of diffraction patterns in order to measure the widths of the projections of grain boundaries. The diffraction patterns were originally measured to construct an orientation map. NMF complements the orientation data with additional information about the width of the projection of the GB plane and the direction of its 2D trace. The main message of this paper is that all that information is extracted from the same diffraction dataset that is already acquired for orientation mapping i.e. no additional images have to be recorded in this method. The inclination of a GB-plane is determined with the help of multiple measurements at different goniometer tilt positions, therefore the crystallographic indices of the GB-plane can be expressed in the reference systems of the neighboring grains. The local thickness of the sample is estimated with reasonable accuracy – the inaccuracy is determined by both the tilt values of the goniometer during the measurements and the diffraction conditions during the data acquisitions. Results given by both the (previous) "manual evaluation" and the "fully programmable" new method are compared in this paper. Thus an automated NMF-evaluation might be a corner stone of a highly improved method in the future, which provides orientation *and* GB-plane statistics on multicrystalline samples.

Acknowledgement

The authors are indebted to S. Nicolopoulos (NanoMEGAS Sprl, Brussels, Belgium) and E. F. Rauch (SIMaP, Grenoble INP/CNRS, France) for providing us the ASTAR hardware and software, respectively. The authors are thankful to A. Eggeman (Department of Materials Science and Metallurgy, University of Cambridge), who called our attention to the application of statistical methods on diffraction data. We are also thankful to A. Jakab for sample preparation and to J. Szívós and L. Illés for their help during the experimental work. The

For Peer Review

GB-plane projection width from diffraction data

Hungarian National Scientific Research Fund (OTKA) supported this work through Grant No. K108869.

References

BERRY M. W., BROWNE M., LANGVILLE A. N., PAUCA V. P. & PLEMMONS R. J. (2007). Algorithms and applications for approximate nonnegative matrix factorization. *Computational Statistics & Data Analysis* 52, 155 – 173.

BRUNET, J-P., TAMAYO, P., GOLUB, T. R. & MESIROV, J. P. (2004). Metagenes and molecular pattern discovery using matrix factorization. In *Proceedings of the national academy of sciences* 101(12), 4164-4169.

Buciu, I., Pitas, I. (2004). Application of non-negative and local non negative matrix factorization to facial expression recognition. In *Proceedings of the 17th International Conference on Pattern Recognition.* 1, 288-291.

DEVARAJAN, K. (2008). Nonnegative matrix factorization: An analytical and interpretive tool in computational biology. *PLoS Computational Biology* 4 (7), e1000029

EGERTON, R. F. (2011). *Electron energy-loss spectroscopy in the electron microscope*, Third edition, New York, Dordrecht, Heidelberg, London: Springer Science+Business Media

EGGEMAN, A. S., KRAKOW, R. & MIDGLEY, P. A. (2015). Scanning precession electron tomography for three dimensional nanoscale orientation imaging and crystallographic analysis. *Nature Communications* 6, DOI: 10.1038/ncomms8267

FORWOOD, C. T. & CLAREBROUGH, L. M. (1991). *Electron microscopy of interfaces in metals and Alloys*, p. 113. Figure 4.8. Bristol, New York: IOP Publishing

GRIMMER, H., BOLLMANN, W. & WARRINGTON, D. H. (1974). Coincidence-site lattices and complete pattern-shift in cubic crystals. *Acta Crystallographica* A 30, 197-207.

For Peer Review

For review purposes only

GB-plane projection width from diffraction data

Kelly, P. M., Jostsons, A., Blake, R. G. & Napier, J. G. (1975). The determination of foil thickness by scanning transmission electron microscopy. *Physica Status Solidi* 31 (2), 771-780.

Kiss, Á. K., Rauch, E. F., Pécz, B., Szívós, J. & Lábár, J. L. (2015). A tool for local thickness determination and grain boundary characterization by CTEM and HRTEM techniques, *Microsc. Microanal.* 21, 422-435.

Kiss, Á. K. & Lábár, J. L. (2013). A method for complete characterization of the macroscopic geometry of grain boundaries. *Materials Science Forum* 729, 97-102.

Lábár, J. L., Kiss, Á. K., Christiansen, S. & Falk, F. (2012). Characterization of Grain Boundary Geometry in the TEM, exemplified in Si thin films. *Solid State Phenomena* 186, 7-12.

Lee D. D. & Seung H. S. (1999). Learning the parts of objects by non-negative matrix factorization. *Nature* 401 (6755), 788-791.

Lee D. D. & Seung H. S. (2001). Algorithms for non-negative matrix factorization. In *Advances in Neural Information Processing Systems 13*, Leen, T.K., Dietterich, T.G. & Tresp, V. (Eds.),~~ pp. ~~556-562.

Lin, C.-J. (2007). Projected gradient methods for non-negative matrix factorization. *Neural Computation*, 19, 2007, 2756-2779.

Midgley, P. A. & Dunin-borkowski, R. E. (2009). Electron tomography and holography in materials science. *Nature Materials* Vol.8, 2009, 271-280.

Paatero, P. & Tapper, U. (1994). Positive matrix factorization: a non-negative factor model with optimal utilization of error estimates of data values. *Environmetrics* 5, 111–126.

For Peer Review

GB-plane projection width from diffraction data

POZSGAI, I. (1997). The determination of foil thickness by scanning transmission electron microscopy. *Ultramicroscopy* 68 (1), 69–75.

RANDLE, V. (1993). *The Measurement of Grain Boundary Geometry*, London: The Institute of Physics Publishing

RANDLE, V. (2001). A methodology for grain boundary plane assessment by single-section trace analysis. *Scripta materiala* 44, 2789–2794.

RAUCH, E. F., VÉRON, M., PORTILLO, J., BULTREYS, D., MANIETTE, Y. & NICOLOPOULOS, S. (2008). Automatic crystal orientation and phase mapping in TEM by precession diffraction. *Microscopy and Analysis* 22 (6), S5-S8.

SAYLOR, D. M., MORAWIEC, A. & ROHRER, G. S. (2003). Distribution of grain boundaries in magnesia as a function of five macroscopic parameters. Acta Materialia 51, 3663–3674.

SAYLOR, D. M., EL-DASHER, B. S., ADAMS, B. L. & ROHRER, G. S. (2004). Measuring the five-parameter grain-boundary distribution from observations of planar sections. *Metallurgical and Materials Transactions* A, 35A, 1981-1989.

SMARAGDIS, P. & BROWN, J. C. (2003). Non-negative matrix factorization for polyphonic music transcription, *2003 IEEE Workshop on Applications of Signal Processing to Audio and Acoustics*, 177-180.

SOTIRAS, A., RESNICK, S. M. & DAVATZIKOS, C. (2015). Finding imaging patterns of structural covariance via Non-Negative Matrix Factorization. *NeuroImage* 108, 1-16.

STADELMANN, P. A. (1987). EMS – A software package for electron diffraction analysis and HREM image simulation in materials science. *Ultramicroscopy* 21, 131-146.

For Peer Review

GB-plane projection width from diffraction data

ZAEFFERER, S., WRIGHT, S. I. & RAABE, D. (2008). Three-dimensional orientation microscopy in a focused ion beam–scanning electron microscope: a new dimension of microstructure characterization. *Metallurgical and Materials Transactions* A, 39A, 374-389.

For Peer Review

		TILT position (inaccuracy: ±0.5°)	Width of the projection and its standard deviation [nm]	Direction of the GB-projection in the photo plane	Percent of excluded sections in width measurements
manual	1st TILT	-12.3° / 0°	74.8 (± 1.6)	1°	
	2nd TILT	-0.2° / 0°	56.9 (± 1.9)	1.4°	
	3rd TILT	14.2° / 0°	23.7(± 1.3)	2.7°	
NMF	1st TILT	-14.7° / 0°	78.3 (± 12.6)	2° (± 0.5°)	9%
	2nd TILT	-2.1° / 0°	60 (± 10.7)	-0.1° (± 1.2°)	15%
	3rd TILT	0° / 2.1°	68.9 (± 5.1)	1.6° (± 0.5°)	6%
	4th TILT	13° / 0°	22.8 (± 5)	2.3° (± 0.6°)	6%

Table 1 *"1st example"*. The main experimental parameters and the primarily determined quantities based on "manual"- and NMF-evaluations

For Peer Review

For review purposes only

	Thickness [nm]	Inclination of the GB-plane	Average direction of the GB-projection	GB-plane according to “upper” grain	GB-plane according to “lower” grain
manual solution	**116.2** (± 8.5)	**65.3°** (± 3.5°)	**1.7°** (± 0.7°)	$\begin{pmatrix}\mathbf{1}\\ \mathbf{1.05}\\ \mathbf{1.02}\end{pmatrix}$	$\begin{pmatrix}\mathbf{1.05}\\ \mathbf{1}\\ \mathbf{1.07}\end{pmatrix}$
	inclination from {111}			**1.2°**	**1.7°**
NMF solution	**151.9** (± 34.9)	**68.3°** (± 11.4°)	**1.5°** (± 1.5°)	$\begin{pmatrix}\mathbf{1.1}\\ \mathbf{1.14}\\ \mathbf{1}\end{pmatrix}$	$\begin{pmatrix}\mathbf{1.17}\\ \mathbf{1}\\ \mathbf{1.06}\end{pmatrix}$
	inclination from {111}			**3.2°**	**3.7°**

Table 2 *“1st example”*. Results for the investigated GB-plane.

For Peer Review

		TILT position (inaccuracy: ±0.5°)	Width of the projection and its standard deviation [nm]	Direction of the GB-projection in the photo plane	Percent of excluded sections in width measurements
manual	1st TILT	-1° / -12.8°	43.6 (± 2.7)	95.2°	
	2nd TILT	0° / -0.2°	21.2 (± 1.9)	94°	
	3rd TILT	-1° / 1°	20.8 (± 1.6)	94.5°	
NMF	1st TILT	-1° / -14.2°	49.8 (± 7)	81.4° (± <0.5°)	3%
	2nd TILT	-1° / -1.5°	23 (± 7.4)	87.2° (± 1.6°)	12%
	3rd TILT	-1° / -2.3°	24 (± 5.6)	86.9° (± <0.5°)	9%
	4th TILT	-1° / -11.1°	27.5 (± 16.1)	88.2° (± 3.7°)	6%

Table 3 *"2nd example"*. The main experimental parameters and the primarily determined quantities based on "manual"- and NMF-evaluations

For Peer Review

For review purposes only

	Thickness [nm]	Inclination of the GB-plane	Average direction of the GB-projection	GB-plane according to “left” grain	GB-plane according to “right” grain
manual solution	**102** (± 6.9)	**78.1°** (± 3.7°)	**94.6°** (± 0.5°)	$\begin{pmatrix}\mathbf{1.11}\\ \mathbf{1}\\ \mathbf{1.1}\end{pmatrix}$	$\begin{pmatrix}\mathbf{1.01}\\ \mathbf{1.04}\\ \mathbf{1}\end{pmatrix}$
			inclination from {111}	**2.5°**	**1°**
NMF solution	**130.3** (± 30.3)	**82°** (± 13.1°)	**83.7°** (± 4°)	$\begin{pmatrix}\mathbf{1.04}\\ \mathbf{1.4}\\ \mathbf{1}\end{pmatrix}$	$\begin{pmatrix}\mathbf{1.56}\\ \mathbf{1}\\ \mathbf{1.51}\end{pmatrix}$
			inclination from {111}	**9°**	**10.6°**

Table 4 *“2nd example”*. Results for the investigated GB-plane.

For Peer Review

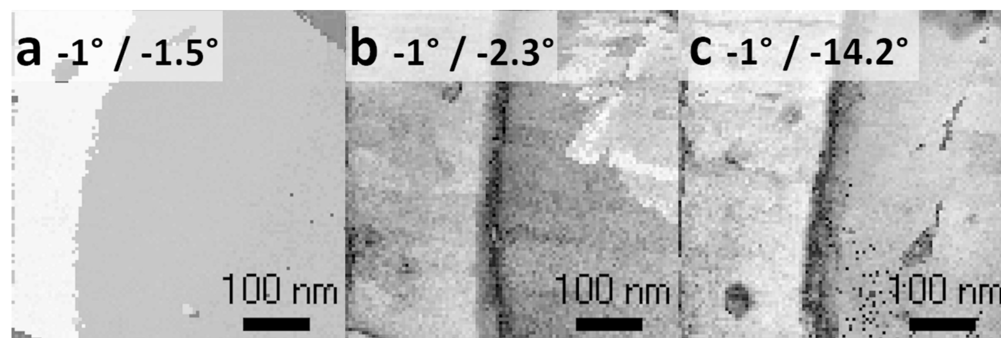

Figure 1. Orientation map (a) and "reliability-maps" (b, c) of the area of interest made at two different tilt positions in our "2nd example". Although the line of the GB appears clearly, none of them is suitable for the measurement of the projected width of the GB-plane.
167x55mm (300 x 300 DPI)

For Peer Review

For review purposes only

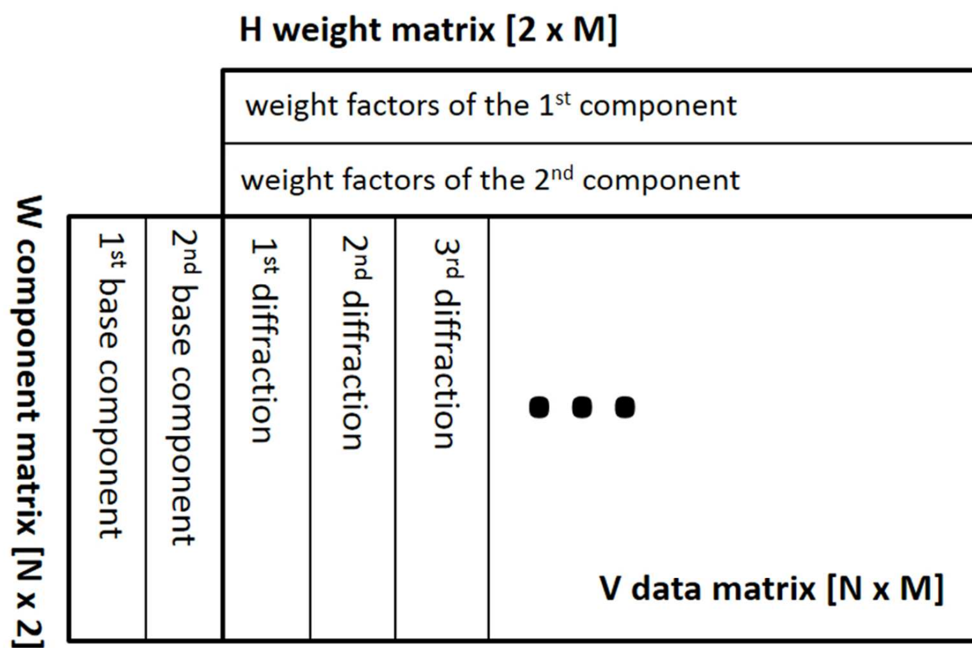

Figure 2. Illustration of the non-negative matrix factorization applied to a set of diffraction patterns.
83x57mm (300 x 300 DPI)

Review

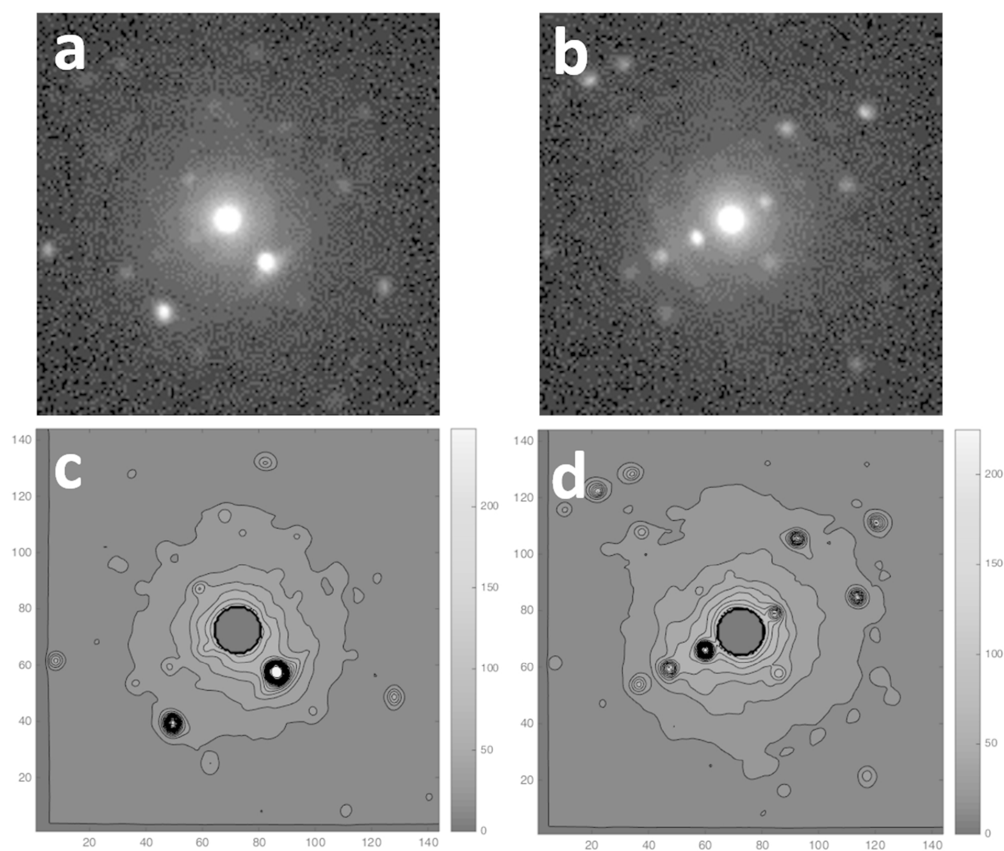

Figure 3. Success of NMF decomposition. Diffraction patterns measured from the centers of the neighboring grains according to the orientation map taken in the “2nd measurement” in the -1° / -14.2° tilt position (a, b). The NMF calculated base components (c, d) unquestionably correspond to the measured ones
167x146mm (300 x 300 DPI)

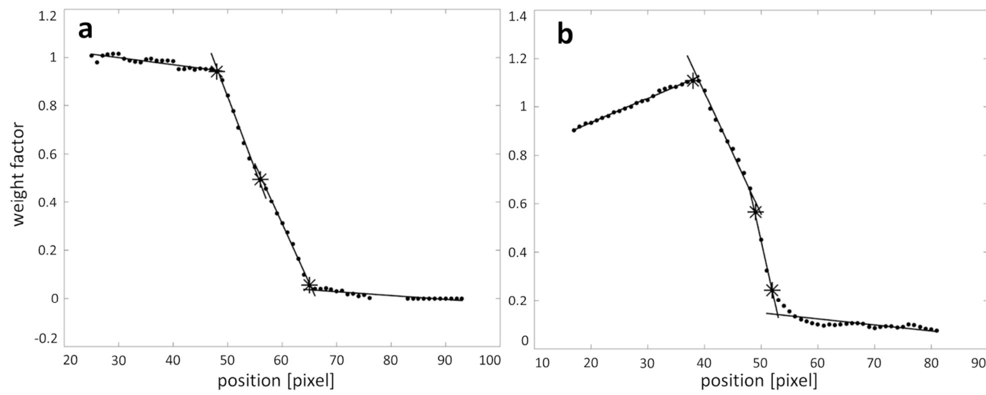

Figure 4. Examples of calculated weight-factors (dots) related to one of the neighboring grains plotted against a line of positions while crossing a GB. a represents the ideal scenario: the transition part is linear, as well as the grain-parts are almost flat, near to 0 and 1. The case shown in b, is more often measured, however that can easily be handled as well. The break-points and the separation point between the “two sides” are marked by asterisks.
167x68mm (300 x 300 DPI)

Peer Review

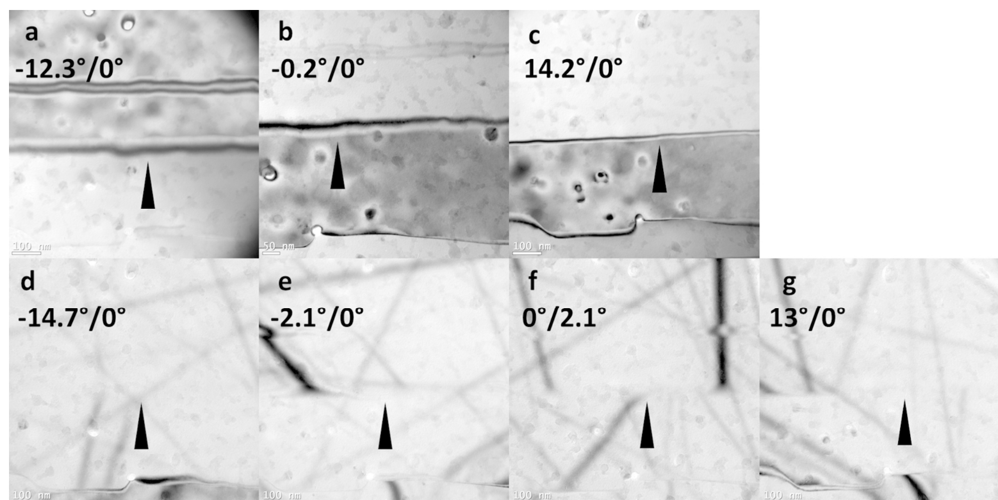

Figure 5. “1st example” Bright field images taken in different tilt positions from a polycrystalline Si thin film. The investigated GB is marked by an arrowhead. The tilt positions are indicated on each image. Sharp thickness fringes are present on a, b and c and different general tilt positions (away from strong diffracting condition) are set in d, e, f and g where the trace of the GB shows no contrast.
167x83mm (300 x 300 DPI)

er Review

For review purposes only

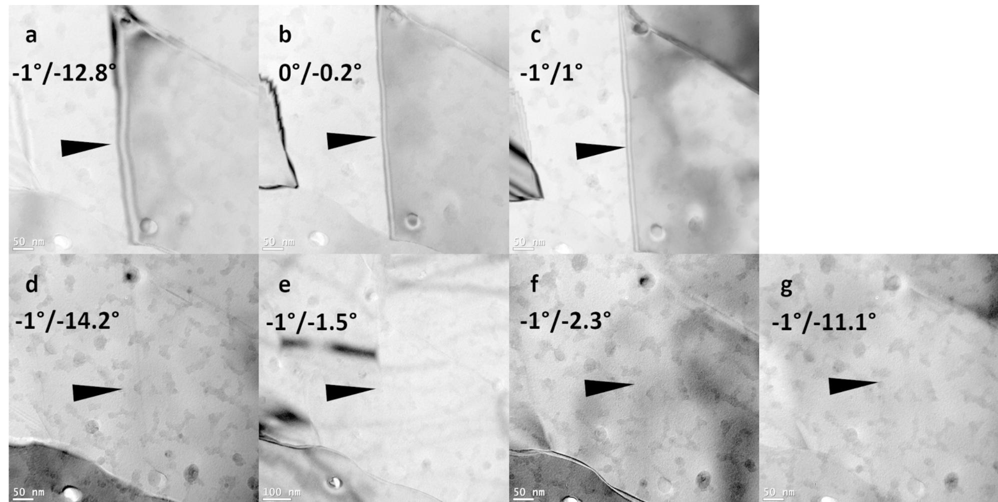

Figure 6. “2nd example” Bright field images taken from a polycrystalline Si thin film in different tilt positions. The investigated GB is marked by an arrowhead. The tilt positions are indicated on each image. Sharp thickness fringes are present on a, b and c and general tilt positions (away from strong diffracting condition) are set in d, e, f and g, where the trace of the GB shows no contrast.
186x92mm (300 x 300 DPI)

er Review

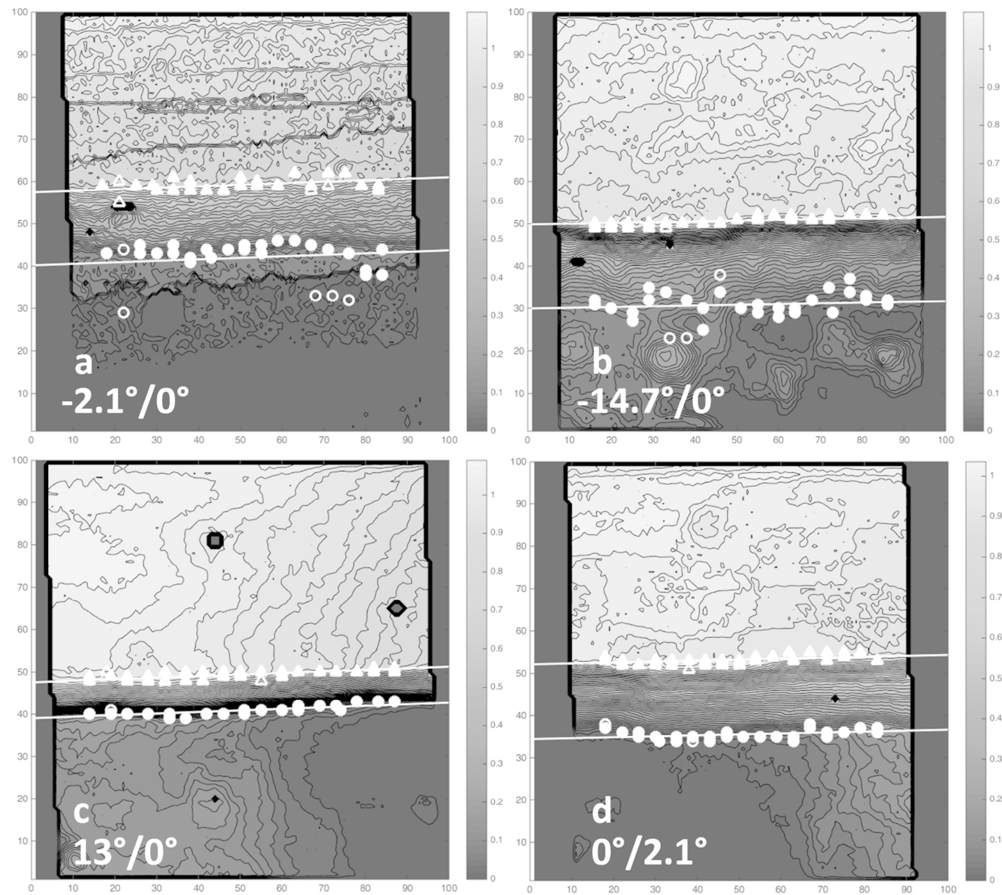

Figure 7. Weight-factors in different tilt positions of the same GB in our "1st example". The GB-projections can be seen very well with the help of the contour-levels; the filled triangles and circles representing the found "break-points" (different symbol for different side of the GB) fit to their edges very well. The straight lines are fitted to the "break-points" on each side with fixed direction (predicted from the orientation map) – the empty symbols show the "break-points" excluded from the evaluation.
167x150mm (300 x 300 DPI)

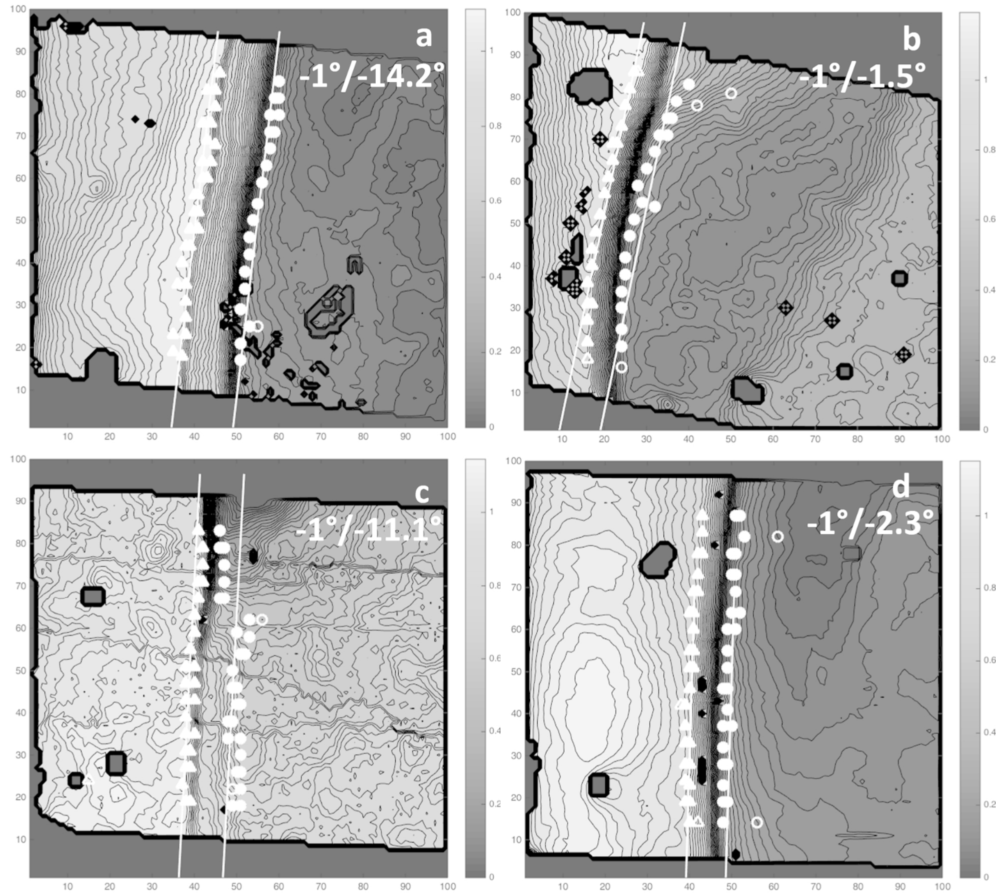

Figure 8. Weight-factors in different tilt positions of the same GB in our "2nd example". The GB-projections can be seen very well with the help of the contour-levels; the filled triangles and circles representing the found "break-points" (different symbol for different side of the GB) fit to their edges very well. The straight lines are fitted to the "break-points" on each side with fixed direction (predicted from the orientation map) – the empty symbols show the "break-points" excluded from the evaluation.
167x150mm (300 x 300 DPI)

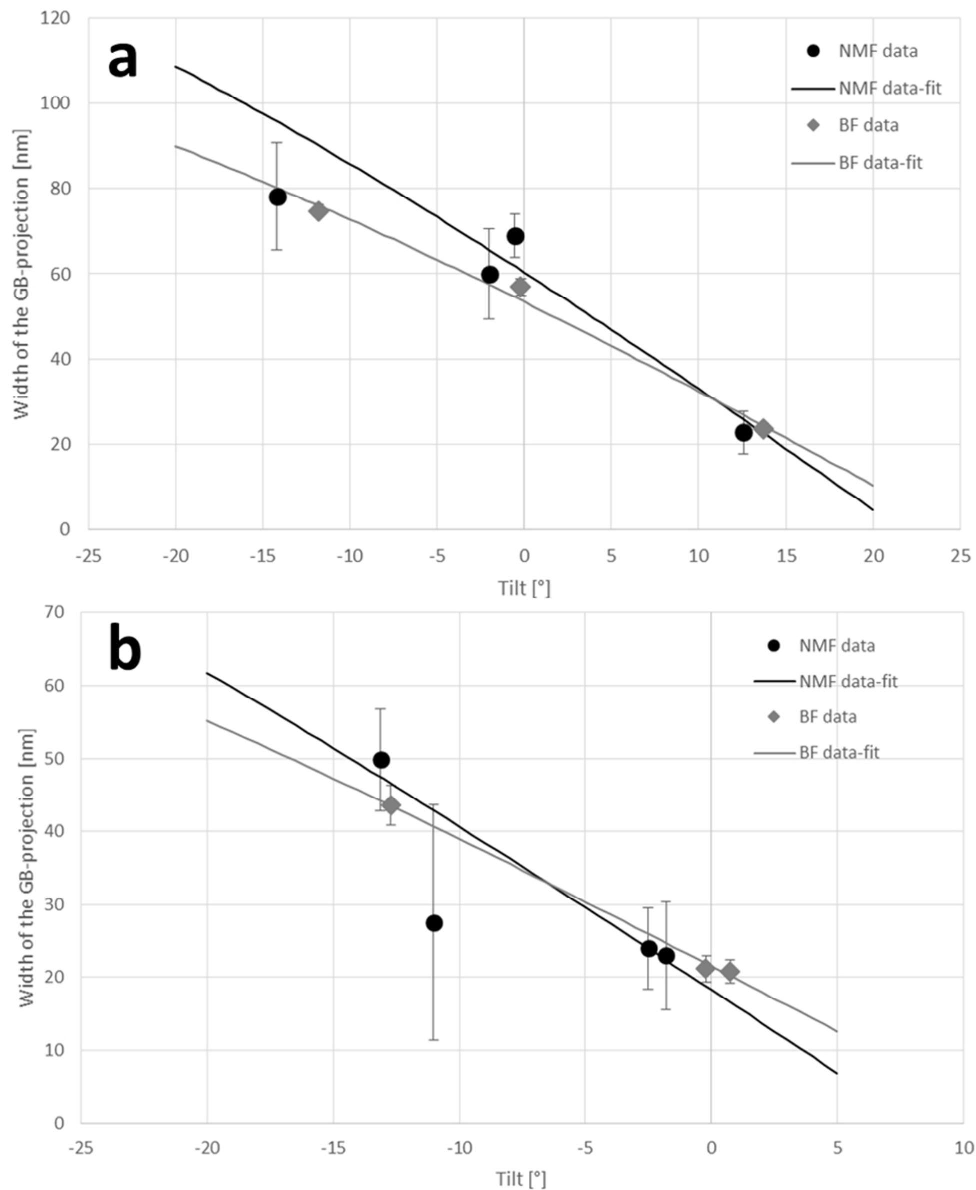

Figure 9. Trigonometric curves are fitted to the data of manual measurements based on bright-field images ("BF data") and NMF-analysis ("NMF data") for the "1st" (a) and the "2nd example" (b). The data given by NMF have significantly bigger errors, however they show the same trends, making possible to calculate the corresponding GB-inclination (i.e. the phase of the fitted cosine – see eq. 3) with similar accuracy.
83x101mm (300 x 300 DPI)

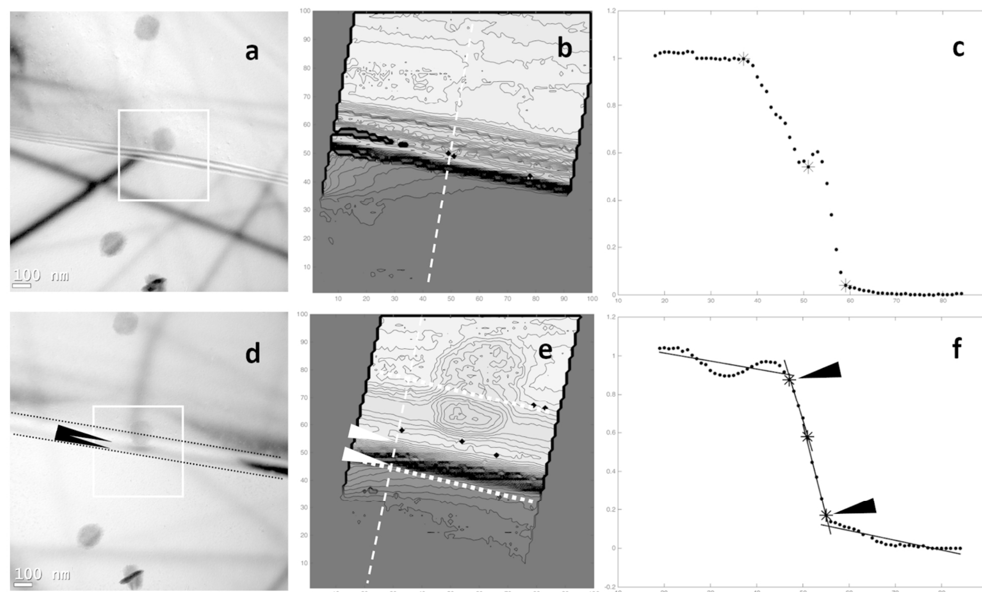

Figure 10. Effect of the presence of thickness-fringes on the weight-factors. The same part of a GB marked by a rectangle in both a and d are analyzed under different two-beam conditions (a-c belong to the first and d-f belong to the second tilt condition). The locations of the sections shown in c and f are marked by thin, white dashed lines in b and e. The same positions are highlighted by arrowheads in d¬ f: the transition shows up in the weight-factors only, where the diffracted spot is strong i.e. the BF image has dark contrast. The edges of the GB-projection are also marked in d and e by thick dashed lines.
167x100mm (300 x 300 DPI)

Review

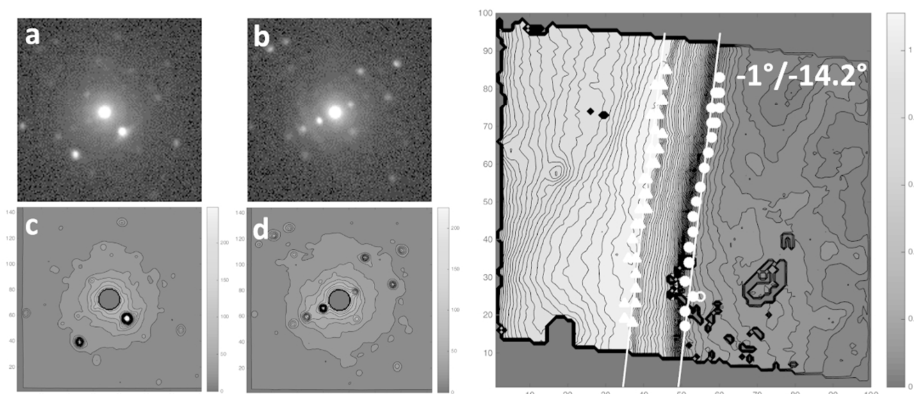

112x44mm (300 x 300 DPI)

For Peer Review